



*1N-32*  
*398376*

# TECHNICAL NOTE

D-1130

## PROJECT ECHO— RECEIVING SYSTEM

E. A. Ohm

Bell Telephone Laboratories

NATIONAL AERONAUTICS AND SPACE ADMINISTRATION  
WASHINGTON

December 1961

•

•

•

•

•

•

## PROJECT ECHO— RECEIVING SYSTEM

By

E. A. Ohm

*Bell Telephone Laboratories*

### SUMMARY

A tracking horn-reflector antenna, a maser preamplifier (and standby parametric preamplifier), and a special FM demodulator were combined to form a low-noise receiving system which made possible the establishment of a high-quality voice circuit via the Echo I passive satellite. This paper describes the 2390-Mc receiving system located at the Bell Telephone Laboratories facility in Holmdel, New Jersey.

## PREFACE

The Project Echo communications experiment was a joint operation by the Goddard Space Flight Center of the National Aeronautics and Space Administration (NASA), the Jet Propulsion Laboratory (JPL), the Naval Research Laboratory (NRL), and the Bell Telephone Laboratories (BTL). The equipment described herein, although designed by BTL as part of its own research and development program, was operated in connection with Project Echo under contract NASW-110 for NASA. Overall technical management of Project Echo was the responsibility of NASA's Goddard Space Flight Center.

## CONTENTS

	Page
Summary . . . . .	i
Preface . . . . .	ii
INTRODUCTION. . . . .	1
RECEIVER DESCRIPTION . . . . .	2
SYSTEM NOISE TEMPERATURE . . . . .	6
Sky . . . . .	6
Antenna . . . . .	7
Waveguide. . . . .	7
Maser . . . . .	12
Converter. . . . .	12
Total System Temperature . . . . .	13
Parametric Amplifier . . . . .	14
FM Demodulator AGC Characteristics. . . . .	14
EXPERIMENTAL RESULTS . . . . .	17
ACKNOWLEDGMENTS . . . . .	18
References . . . . .	19
Appendix A - Front-End Tuning . . . . .	21
Appendix B - System Temperature Measurements . . . . .	23
Appendix C - Sky Temperature. . . . .	24
Appendix D - Liquid Nitrogen . . . . .	26
Appendix E - Liquid Helium. . . . .	28



# PROJECT ECHO— RECEIVING SYSTEM\*

by  
E. A. Ohm

*Bell Telephone Laboratories*

## INTRODUCTION

It was calculated that by using large antennas and a high-powered transmitter, a modest carrier could be received in Holmdel, New Jersey from the Jet Propulsion Laboratory facility in Goldstone Lake, California, by reflection from the Echo I satellite (Reference 1). In order to establish a good voice circuit with this carrier, it was clear that the effects of noise had to be reduced by using a very-low-noise receiver. It was also clear that a special demodulator, which featured FM with negative feedback (Reference 2) could reduce the noise effects still further. Although a parametric amplifier in combination with this type of demodulator would yield a good voice circuit under near-ideal conditions, a maser would allow a circuit with a more practical carrier-to-noise margin.† In this regard, a previous experiment had demonstrated that an ultra-low-noise system temperature could be achieved in practice by using a low-noise horn-reflector antenna in combination with a traveling-wave solid state maser (Reference 3).

In accordance with these preliminary results a larger horn-reflector tracking antenna was combined with two traveling-wave masers — or, alternately, two "standby" parametric amplifiers — to provide two separate low-noise systems, one for each sense of circular polarization. Special FM demodulators with negative feedback were used to achieve voice circuits of excellent quality from the resulting modest carrier-to-noise ratios. In addition Automatic Gain Control (AGC) voltages from the FM demodulator were used to monitor the carrier levels, voltages proportional to the system temperatures but independent of incoming

\*The substance of this paper was published in the Bell System Technical Journal, Vol. XL, no. 4, July 1961. It is republished here, with minor revisions, by permission of Bell Telephone Laboratories.

†It was important to maintain some margin; otherwise, at a critical carrier-to-noise ratio a small decrease in carrier or increase in noise would change the voice circuit from good to completely unintelligible. A discussion of this "threshold" effect is included in a paper by Ruthroff (Reference 2). For the audio circuit used here, the "threshold" ratio of carrier to noise power (referred to a 6-kc band) is 14 db.

carrier levels were derived, and each of these two types of voltages was recorded and calibrated.

The next section describes how the receiver generated useful output information. It is followed by sections on the system noise temperature, the FM demodulator AGC characteristics, and the experimental results.

## RECEIVER DESCRIPTION

A block diagram of the receiving system is shown in Figure 1. Its operation will be explained by describing how each successive block in the diagram acts on the carrier, the noise, or both as it passes through the receiver. (The italicized words in this section refer to blocks labeled in Figure 1.)

Starting on the left, it is assumed that both senses of circularly polarized carrier and noise powers are incident on the antenna. A special significance of the *sky* is that thermal radiation from the atmosphere increases the system noise temperature (Figure 2) as the antenna is lowered toward the horizon. The *horn antenna* focuses the circularly polarized carriers and noise into the *waveguide assembly*, which is shown in Figure 3. There, after passage through a rotating joint, the finline  $\Delta 90^\circ$  section converts the two senses of circular polarizations into orthogonal linear polarizations, and these are further separated by the polarization couplers into separate waveguide channels indicated as the "clockwise" and "counter-clockwise" channels in Figure 3. Two 18-db waveguide directional couplers

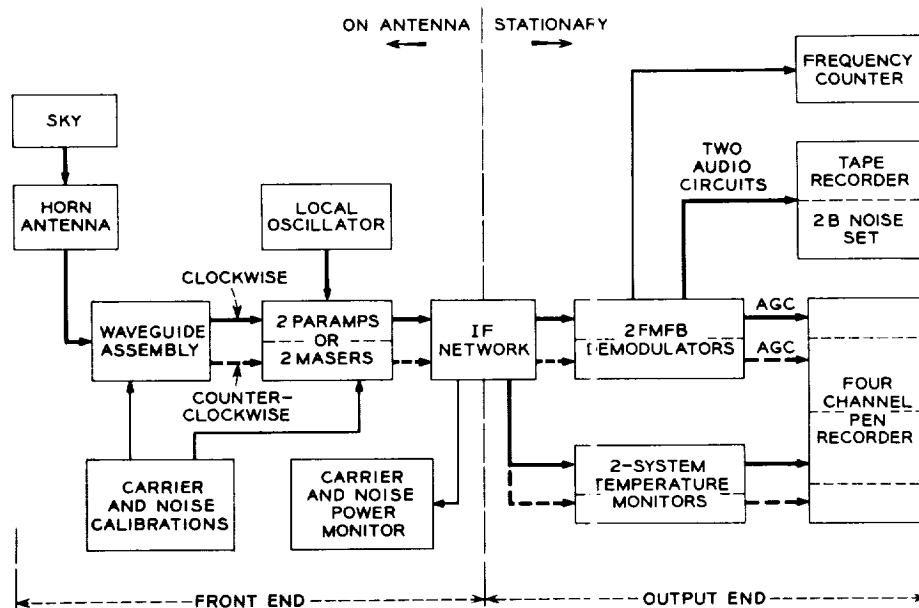


Figure 1 - Block diagram of the Holmdel receiver



are also provided in this region for the convenient insertion of *carrier and noise calibrations* into each channel. From here the two channels were connected via waveguide-to-coaxial transducers to two *maser preamplifiers* or alternatively to two *parametric preamplifiers*. From this point on the channels are completely alike and independent, and therefore only one of them will be discussed.

After sufficient preamplification to nearly eliminate the effects of the noise from the following stages, the carrier and noise powers are heterodyned with a *local oscillator* to an intermediate frequency. The *IF network* further amplifies the carrier and noise to reduce the effects of possible interference, and then transmits this information via the antenna slip ring assembly and long runs of coaxial cable to the "output end" of the receiver. A means for bridging the antenna end of either IF transmission line with a *carrier and noise power monitor* is also provided, so that the "front end" of each channel can be readily tuned and its system temperature measured from inside the antenna cab (see Appendix A).

One output of each IF transmission line is connected to an *FM with negative feedback (FMFB) demodulator*. This unit recovers the audio modulation from the frequency

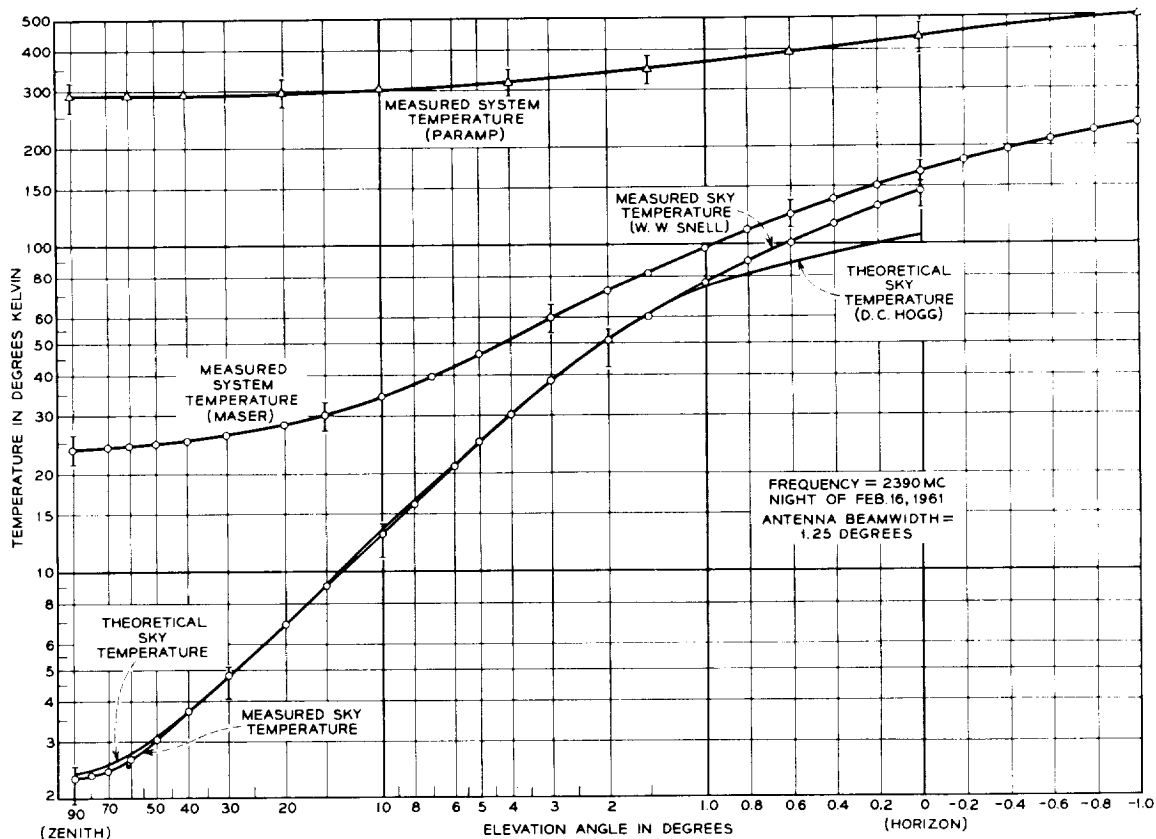


Figure 2 - Measured sky and system temperatures

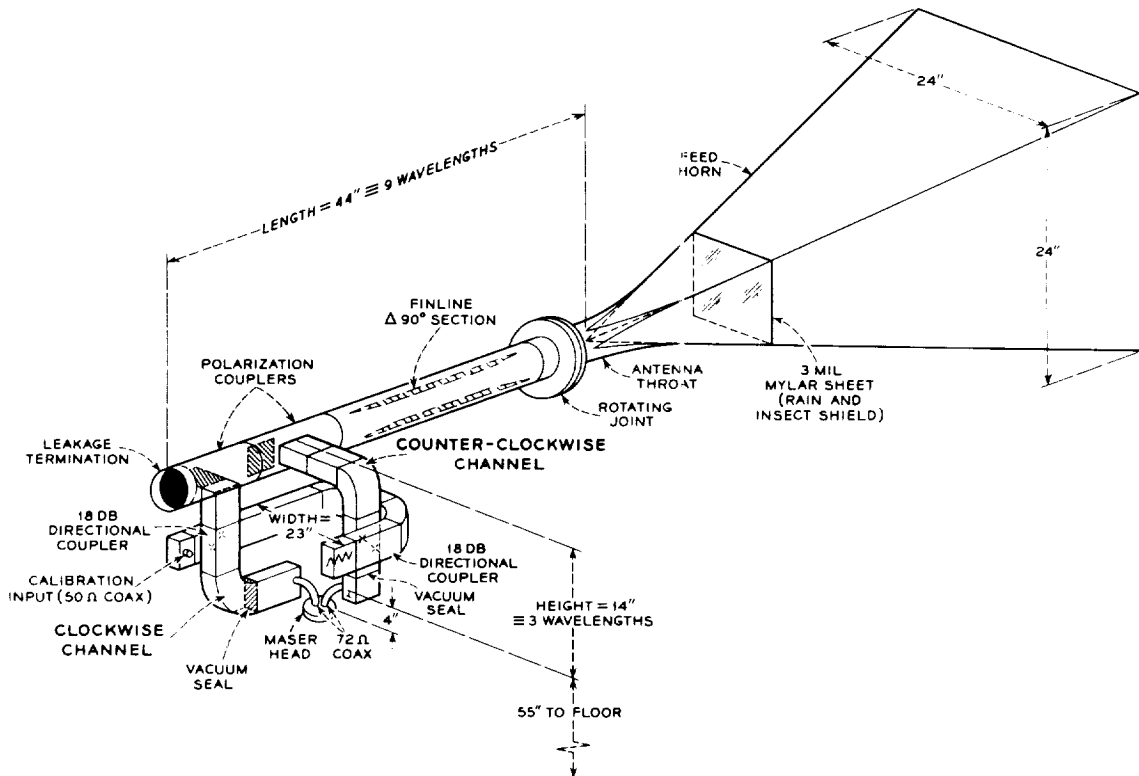


Figure 3 - Waveguide assembly

modulated carrier with the usual FM advantage, but for a much smaller carrier-to-noise ratio than would otherwise be possible. For proper demodulation over a wide range of 70-Mc carriers, the 1.2-Mc input of the FM limiter is held constant with an AGC feedback loop, which is shown in Figure 1 of Reference 2. A sample of this AGC voltage is forwarded to the *recorder*, where a back bias is superimposed in order to display the voltage range of greatest interest. Through the addition of known 2390-Mc carrier powers to the RF input of each channel (via the 18-db waveguide directional couplers) it became practical to calibrate AGC carrier level voltages before and after every pass. Typical recorded AGC voltages are shown in Figure 4, where they are labeled "counter-clockwise channel carrier" (top recording) and "clockwise channel carrier" (third from top).

Thus far it has been tacitly assumed that the carrier and noise bandwidths are identical. Actually the modulated carriers, including Doppler shifts, occupy only a small portion of the "front-end" bandwidth, as is shown in the center of Figure 5; this permits the use of a simple circuit that can continuously monitor the system temperature while carriers are also being received. By assuming constant gain, it can be shown that the output noise from any slice of the "front-end" bandwidth is proportional to the system temperature.

13-1100

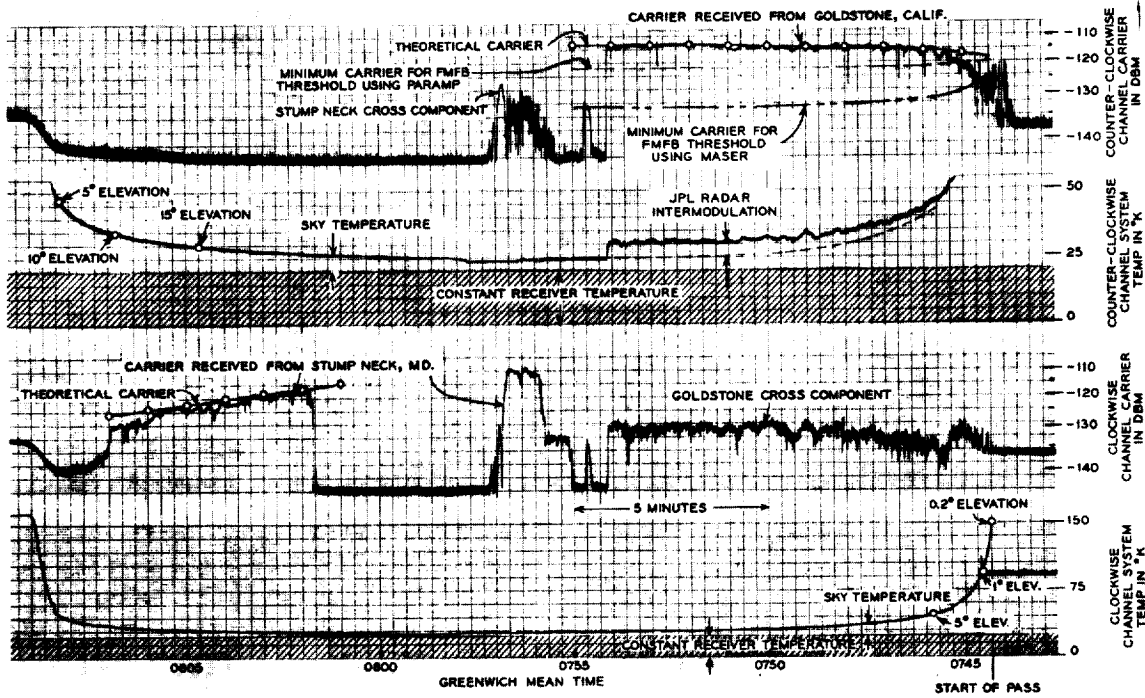


Figure 4 - Typical Project Echo receiver recordings (for Pass 60, August 17, 1960)

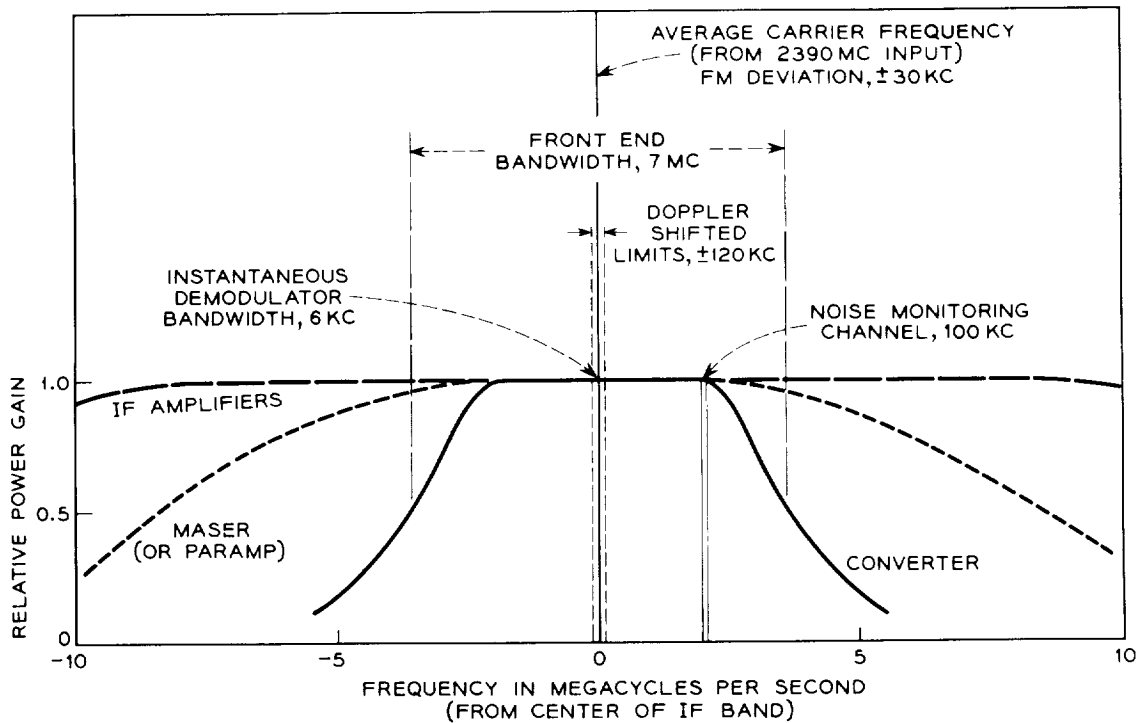


Figure 5 - Receiver bandwidths

In order to eliminate carrier interference, the noise temperature monitoring channel was chosen as far from the carrier frequency as is practical (Figure 5).

A second output of each IF transmission line is accordingly connected to a *system temperature monitor* (Figure 1), where the required selectivity is achieved by using a very narrow-band IF amplifier. By following this with a precision square-law detector, a dc output voltage proportional to the system temperature is obtained. To calibrate this output voltage a known amount of excess noise from a standard noise lamp is added to the input waveguide via the 18-db directional couplers shown in Figure 3. The resulting calibrated voltages, which indicate system temperature, are shown in Figure 4, where they are labeled "counter-clockwise channel system temperature" (second from top) and "clockwise channel system temperature" (bottom recording).

The *frequency counter* output was used to tune the FM demodulators in the presence of large Doppler shifts, and the *2B noise set* was used to verify the quality of the satellite system voice circuits.

Thus the useful receiver outputs are two audio circuits, one for each sense of circular polarization, and a set of four calibrated voltage records, which represent the received carrier powers and noise temperatures for each polarization. These recordings, which may be also seen in Figures 10 through 21 of Reference 4, provide a continuous description as to how the west-to-east satellite system was operating.

## SYSTEM NOISE TEMPERATURE

The sky, antenna, waveguide, maser, and converter all made significant contributions to the system noise temperature. This section shows by the use of measurements, calculations, or reasonable estimates, how much temperature was added by each of these sources. The sum of these temperatures is found to be in fair agreement with measurements of the overall system temperature. Details of the overall system measurements are given in Appendix B.

### Sky

Since the background sky temperature, which varies with the antenna elevation angle, is always observed by a satellite-tracking antenna, it is necessary to include it as a part of the system noise temperature. The sky temperature contribution (measured as shown in Appendix C) is only 2.3°K at the zenith but increases to 25°K when the antenna is lowered to a five-degree elevation (Figure 2). Thus, in order to design a system which will work down to this elevation, about 23°K must be added to the system temperature at the

zenith. Closer than five degrees to the horizon the sky temperature increases even more rapidly, and it becomes progressively difficult to provide a system for satellite communications. Fortunately the higher temperatures are only present for a small portion of a pass, as is shown by the typical system temperature recordings of Figure 4. Although communications cannot typically be maintained close to the horizon, this time can be well spent in acquiring the satellite and making preliminary carrier-level measurements.

There are additional isolated sources of sky temperature; but they are few and are not usually encountered during a satellite pass. The sun, however, which has a temperature of  $40,000^{\circ}\text{K}$  at 3 kMc, can add about  $4000^{\circ}\text{K}$  via the main beam of the antenna. (The added temperature is less than the sun's temperature because the antenna beamwidth, about 1.25 degrees in this case, is greater than the 0.5 degree angle subtended by the sun. The sun was also observed to add from  $5^{\circ}$  to  $20^{\circ}\text{K}$  via various side lobes. Via the main beam the hottest radio star, Cassiopeia A, was found to add  $14.3^{\circ}\text{K}$ , the moon about  $16^{\circ}\text{K}$ , and the center of the galaxy  $4.5^{\circ}\text{K}$ . For a more uniform sky temperature reference, an antenna should be pointed about 14 degrees south of the zenith, a region traversed by fewer and cooler radio stars.

## Antenna

The tracking horn antenna is described in Reference 5. It is similar to those used for microwave radio relay, its main advantage for a low-noise system being the exceedingly low back and side lobes,\* which reduce interference and are estimated to add only  $2 \pm 1^{\circ}\text{K}$  to the system temperature. This estimate is based on temperature "not otherwise accounted for" in a previous experiment (Reference 3); it is somewhat larger than the calculated temperature expected from back lobes measured on a similar antenna.

A second advantage of this antenna is that a long waveguide run, which adds to the system temperature, is not required. A third advantage is that the way this antenna can be mounted (Reference 5) makes it convenient to provide a shielded laboratory for the preamplifiers and associated receiving equipment.

## Waveguide

The purpose of the waveguide assembly is to transmit the received circularly polarized energy from the antenna to the preamplifiers with a minimum of added noise. The

---

\*Although the side lobes near the main beam are not as small, they are usually pointed toward the cold sky, and therefore do not add much to system temperature. This is confirmed in Figure 2 by the close agreement between the measured and theoretical sky temperatures. As can be seen, the agreement is good from the zenith down to an elevation angle of  $1-1/2$  degrees.

waveguide assembly is shown in Figure 3 and its general operation has already been described. Since each 0.1 db of insertion loss adds about  $7^{\circ}\text{K}$  to the system temperature, it was advantageous to minimize waveguide losses. Broadband components are used throughout in order to minimize the use of "lossy" tuning devices. The possibilities of significant resonance losses were eliminated by adjusting each component to have a return loss of 35 db or greater over a 100-Mc bandwidth. In addition, all parts were made as short as was practical. A summary of the loss of each waveguide component is given in Table 1 in terms of the equivalent increase in system temperature, or "loss temperature." The unique features of the waveguide assembly are discussed below.

The most important practical aspect of the waveguide assembly is the rotating joint, which allows the antenna to rotate in elevation. This eliminated the need for designing equipment to swing  $\pm 45$  degrees with the antenna elevation. The rest of the receiver is connected solidly to the floor of the antenna cab.

A cross section of the rotating joint is shown in Figure 6. The purpose of the multiple chokes is to reduce the insertion loss and also to greatly reduce leakage from the antenna cab calibration equipment into the receiver front end. On the assumption of high (free space) impedance at the outer edge, all lengths were adjusted to give the minimum impedance at the inner surface of the waveguide.  $L_1$ ,  $L_3$ , and  $L_5$  were found from Schelkunoff's analysis (Reference 6) of cylindrical cavity resonators. As shown by Mumford (Reference 7), the desired lengths are somewhat shorter than a quarter wavelength, owing to the greater capacitive loading at the smaller radii.  $L_2$  and  $L_4$  were adjusted to resonate with  $L_1$  and  $L_3$ , assuming excitation of the  $\text{TE}_{01}$  coaxial mode (Reference 6), which is also shown in Figure 6.

The total measured loss temperature of the rotating joint assembly is only  $0.14 \pm 0.02^{\circ}\text{K}$ . For comparison purposes, the loss temperature of a simple choke, also shown in Figure 6, is about  $1^{\circ}\text{K}$  using dominant-mode waveguide, and about  $0.4^{\circ}\text{K}$  using oversize waveguide which has a diameter of 1.4 wavelength. The nominal 20-mil gap is adequate to allow for residual mechanical distortions of the supporting structure. Loss temperature increased about 15 percent because of the 15-mil offsets of the rotating portion of the joint. These offsets are due to the slightly eccentric rotation of the antenna throat.

The waveguide assembly also acts as a circular polarization filter, since it separates the two senses of incident circular polarization. Any circularly polarized wave can be thought of as two linear waves at right angles in space and displaced 90 degrees in time phase from each other, as shown at the top of Figure 7. An observer at A would see a wave that rotates in the counter-clockwise direction. If wave 1 is retarded a quarter-wavelength or 90 degrees with finline (or other) loading, a vertically polarized wave will result. Similarly, if 1 had been lagging wave 2, instead of leading, the observer at A would have seen a clockwise rotation. If wave 1 is now retarded 90 degrees by the same finline, wave 2 and wave 1 will be lined up. The result is a horizontally polarized wave.

Thus the counter-clockwise wave is transformed to vertical, and the clockwise wave to horizontal linear polarization, by the 90-degree retardation of one linear component. This finline  $\Delta 90$  degree component was designed with only a modest fin penetration, as is shown at the bottom of Figure 7, in order to keep the insertion loss low and reduce the residual mismatch. The required match was achieved by dividing each fin taper length into three  $\lambda_g/4$  segments and adjusting the slopes of these three consecutive segments to be in the ratio of  $1:\sqrt{2}:1$  (this ratio was found, empirically, to give the best broadband match). The measured relative phase shift was  $90 \pm 1$  degrees at 2390 Mc. The power coupled from one channel to the other is down at least 40 db, owing to the  $\pm 1$  degree tolerance.

The pertinent details of the polarization coupler are shown in Figure 8. Because of the unique triangular plates, the return loss of the "straight-through" polarization was

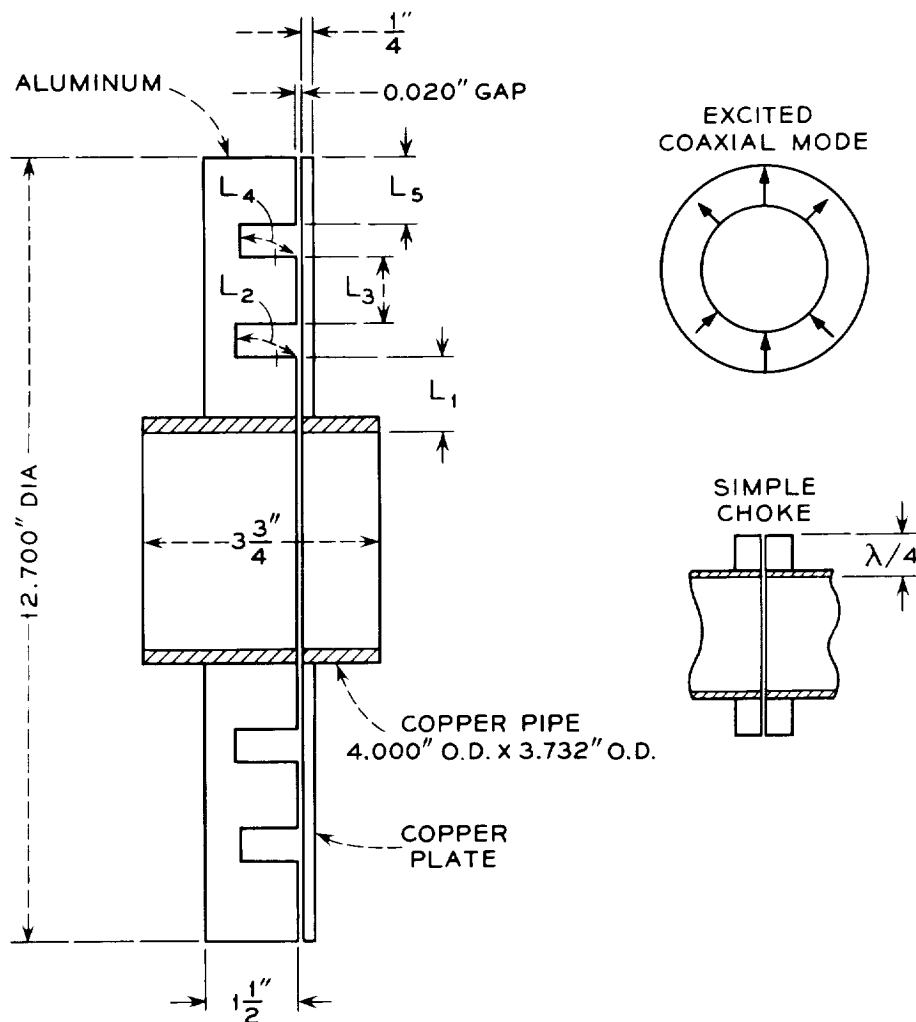


Figure 6 - Rotating joint

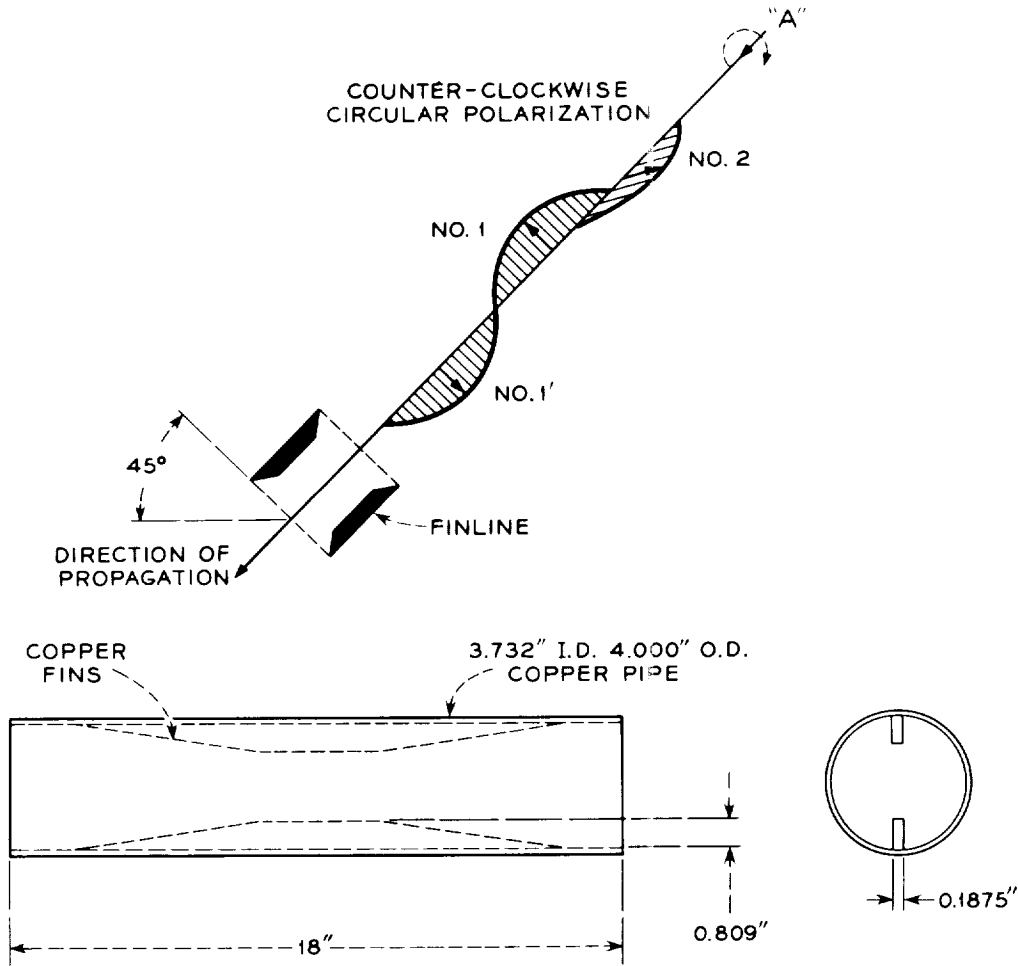


Figure 7 - Finline 90-degree section

greater than 40 db over many octaves. There is some power cross-coupled from one polarization to the other because of small mechanical asymmetries, but this is also down at least 40 db.

The polarization filter consists of the finline in combination with the adjacent polarization coupler oriented as shown in Figure 3. After allowing for arbitrary phasing of the above couplings, and since the rotating joint and antenna throat are fairly symmetrical, it appears that the total power that can be coupled from one channel to the other (via the waveguide) must be down at least 34 db.

The cross sections of the antenna throat were varied smoothly in order to give a "raised cosine" distribution of reflection coefficient per unit of waveguide wavelength. As for the slopes of this antenna feed horn, about three wavelengths are required to go from the constant impedance of free space to that of the dominant mode waveguide



(a ratio of 1.7 to 1). Bolinder (Reference 8) shows that the theoretical return loss for this length is a respectable 67 db. Therefore this well-matched electroformed throat turned out to have an excess length (i.e., beyond the apex of the antenna throat) of only half a wavelength. Assuming an increased loss factor of 1.25 for surface roughness of electroformed copper (Reference 9), the temperature contribution of this component was calculated to be  $0.33 \pm 0.05^\circ\text{K}$ .

Because of its near-minimum attenuation constant, a 72-ohm characteristic impedance was chosen for the maser input coaxial line. The coaxial probe of the waveguide-to-coaxial transducer was otherwise conventional, but it had to be carefully adjusted in length and location to achieve the lowest possible insertion loss. Another feature of this component was a new location for the maser vacuum seal. It was moved from a cold location in the coaxial line to the much warmer waveguide connecting flange in order to prevent increased loss from water condensation. The seal itself is an 11-mil sheet of Mylar cemented in a countersunk flange with a special adhesive. The outer wall of the coaxial line was connected to the transducer with a commercial flare fitting. This provided an excellent vacuum connection when used with a thin soft-copper flared-washer seal and it made it possible to disconnect the maser quickly for an emergency switch to the parametric amplifier.

The measured coupling of the conventional cross-guide coupler is  $18.15 \pm 0.15$  db. The loss temperature due to the insertion loss is:

$$T^\circ\text{K} = \frac{290}{\text{antilog} \frac{\text{db}_{\text{coupling}}}{10}}$$

The loss temperature in this case is  $4.45 \pm 15^\circ\text{K}$ . When a parametric amplifier is used, an 18-db coupling is needed to add sufficient noise from an argon lamp for a system temperature measurement. The wall loss adds about  $0.20^\circ \pm 0.02^\circ\text{K}$ , for a total loss temperature of  $4.65 \pm 0.17^\circ\text{K}$ . With only a maser system the coupling could be reduced to 27 db and the corresponding loss temperature would then be a less objectionable  $0.8^\circ\text{K}$ . For the Echo experiments the 18-db couplers were retained in order to allow a faster change-over to the standby parametric amplifiers.

The loss temperatures of many of the waveguide parts were calculated, using the measured attenuation constants of the round and rectangular waveguides. These calculations include estimates, when necessary, for the somewhat higher insertion losses due to

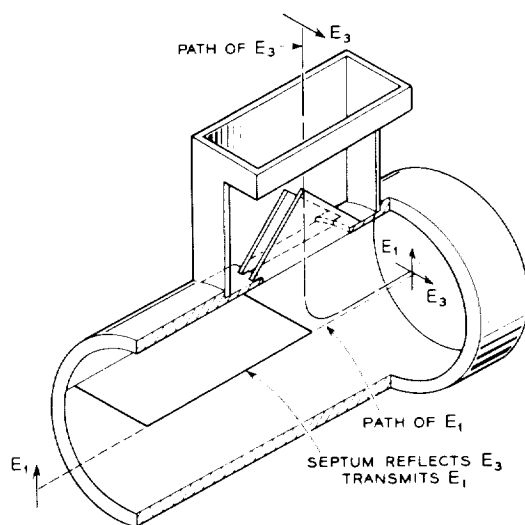


Figure 8 - Polarization coupler

"greater than dominant mode" wall current densities. The loss temperatures of all the waveguide parts are summarized in Table 1.

Table 1  
Waveguide Sources of System Temperature

Source	Counter-Clockwise Channel	Clockwise Channel	Remarks
Throat	$0.33 \pm 0.05^\circ\text{K}$	$0.33 \pm 0.05^\circ\text{K}$	calculated
Rotating joint	$0.14 \pm 0.02^\circ\text{K}$	$0.14 \pm 0.02^\circ\text{K}$	measured
Finline	$0.46 \pm 0.06^\circ\text{K}$	$0.46 \pm 0.06^\circ\text{K}$	calculated
Polarization coupler (bend)	$0.48 \pm 0.05^\circ\text{K}$	$0.48 \pm 0.05^\circ\text{K}$	measured
Polarization coupler (straight)		$0.23 \pm 0.04^\circ\text{K}$	calculated
Rectangular waveguide	$0.19 \pm 0.02^\circ\text{K}$		calculated
Directional couplers	$4.65 \pm 0.17^\circ\text{K}$	$4.65 \pm 0.17^\circ\text{K}$	calculated
E-plane bend	$0.25 \pm 0.03^\circ\text{K}$		calculated
H-plane bend		$0.27 \pm 0.03^\circ\text{K}$	measured
Waveguide-to-coaxial transducer	$0.50 \pm 0.25^\circ\text{K}$	$0.50 \pm 0.25^\circ\text{K}$	measured
Predicted total	$7.00 \pm 0.65^\circ\text{K}$	$7.06 \pm 0.67^\circ\text{K}$	

The total loss temperature of the waveguide could be reduced about  $0.5^\circ\text{K}$  by using higher conductivity copper (commercially available) in place of the red brass used for the rectangular parts and arsenical copper used for the round parts.

## Maser

The maser low-noise preamplifier assembly has been described in Reference 10. It had the ability to amplify the incoming carrier and noise more than 36 db without adding more than  $8^\circ\text{K}$  to the system temperature. The large gain was required in order to reduce greatly the system temperature contribution from the converter. The gain was also very stable-an important factor in keeping the receiving system properly calibrated. The variation, during a half-hour period, from the initial input carrier level calibration before a satellite pass until the recheck after the pass, was typically only a few tenths of a decibel.

The outer dewar of the maser had to be cooled by a liquid nitrogen system and the inner dewar by a liquid helium system; these cooling techniques are discussed in Appendixes D and E.

## Converter

Since the converter system temperature contribution (referred to the amplifier input) is the converter temperature reduced by the net gain from the input, a low noise figure was required. Because the maser saturation threshold occurs at an output level of  $-40\text{ dbm}$ , low leakage from the local oscillator was also desirable. To meet these requirements a

balanced converter using 1N263 diodes was designed by R. H. Turrin. It had a noise figure of 7.5 db (1300°K) and local oscillator leakage power on the order of -20 dbm. The leakage power was further reduced to -47 dbm with a coaxial isolator. Since the additional loss between the maser and converter was 2.3 db (1.35 db for interconnecting coax, 0.75 db for the isolator, and 0.2 db for a monitoring directional coupler) and the maser gain was 36.3 db, the net gain from the input was reduced to 34 db. The temperature contribution of the converter system was therefore calculated to be  $0.6 \pm 0.15^\circ\text{K}$ . The limits are due mainly to measured day to day changes of the maser gain.

## Total System Temperature

A rough idea of the total system temperature was found by adding together the contributions of all of the known sources, as is shown in Table 2.

The total system temperature was also measured by using the noise-lamp technique which is discussed in Appendix B. By this method the temperature was found to vary a few degrees from day to day, but the lowest temperature was consistently  $22.2 \pm 2.2^\circ\text{K}$ . By realistically assuming that all sources were then contributing their fair share (as is also tacitly assumed in Table 2) it is possible to improve the overall accuracy. The actual minimum system temperature must be in the overlap region of the measured results of appendix B and the total results of Table 2, namely, between  $20^\circ$  and  $22.1^\circ\text{K}$ . The most likely minimum system temperature is therefore:

$$T_{\text{system}} = 21 \pm 1^\circ\text{K}.$$

The inference from this result is that the "+" temperature possibilities of Table 2 must predominate.

Table 2  
Sources of System Temperature

Source	Temperature
Sky (at zenith)	$2.30 \pm 0.20^\circ\text{K}$
Horn Antenna	$2.00 \pm 1.00^\circ\text{K}$
Waveguide (counter-clockwise channel)	$7.30 \pm 0.65^\circ\text{K}$
Maser assembly	$7.00 \pm 1.00^\circ\text{K}$
Converter	$0.50 \pm 0.15^\circ\text{K}$
Predicted total system temperature	$19.10 \pm 3.00^\circ\text{K}$

## Parametric Amplifier

The fairly low noise "standby" parametric preamplifier has been described in Reference 11. The receiving system was designed so that the "paramp" could be switched into the system, tuned, and calibrated in about 15 minutes. The chief effect of using it in place of the maser was to increase the minimum system temperature to 290°K. The resulting temperatures for all angles of antenna beam elevation are shown by the upper curve in Figure 2. During a pass the paramp gain usually decreased about a decibel, and this turned out to be a limiting factor in the received carrier calibration accuracy.

## FM Demodulator AGC Characteristics

The FM features of the FM demodulator are discussed by Ruthroff in Reference 2. The purpose of the present discussion is to show how the AGC voltage features were exploited in order to obtain accurate recordings of the 2390-Mc received carrier power.

A simplified block diagram of the FM demodulator (Figure 1 of Reference 2) shows that there are two feedback loops; one for FM and the other for AGC. The purpose of the FM loop is to make the voltage-controlled oscillator (VCO) frequency track the FM deviations of the input carrier. The primary purpose of the AGC loop is to keep the 1.2-Mc carrier amplitude at the limiter input fairly constant over a wide range of input power. The secondary purpose is to calibrate the AGC voltage as a function of known 2390-Mc input carriers and, conversely, to deduce the input levels from AGC voltages generated by the actual received carriers.

Since the AGC voltage is derived from the amplitude of the carrier and/or AM noise in the path common to both feedback loops, it is also a function of the FM demodulation process. It turns out that the maximum AGC voltage is always obtained when the FM demodulator is "tuned" by properly adjusting the VCO frequency. It was found that the audio circuit quality for strong carriers was always improved by maximizing the AGC voltage; for weak carriers, i.e., those below the FM threshold, it was found that erratic AGC voltages could be readily maximized by using audio quieting as a tuning aid.

A practical feature of the demodulator was that all tuning was readily accomplished with a single control. This made it possible to calibrate just before and after each pass to decrease long-term drift errors. Aided by the VCO frequency counter, this also made it possible to acquire readily and track accurately the received carriers despite Doppler shifts of  $\pm 90$  kc. The implication of this experiment was that automatic frequency tracking could and should be provided for future satellite receivers.

A typical FM demodulator AGC characteristic is shown in the right-hand curve of Figure 9. The known 2390-Mc carriers were inserted via the waveguide couplers after

D-1130

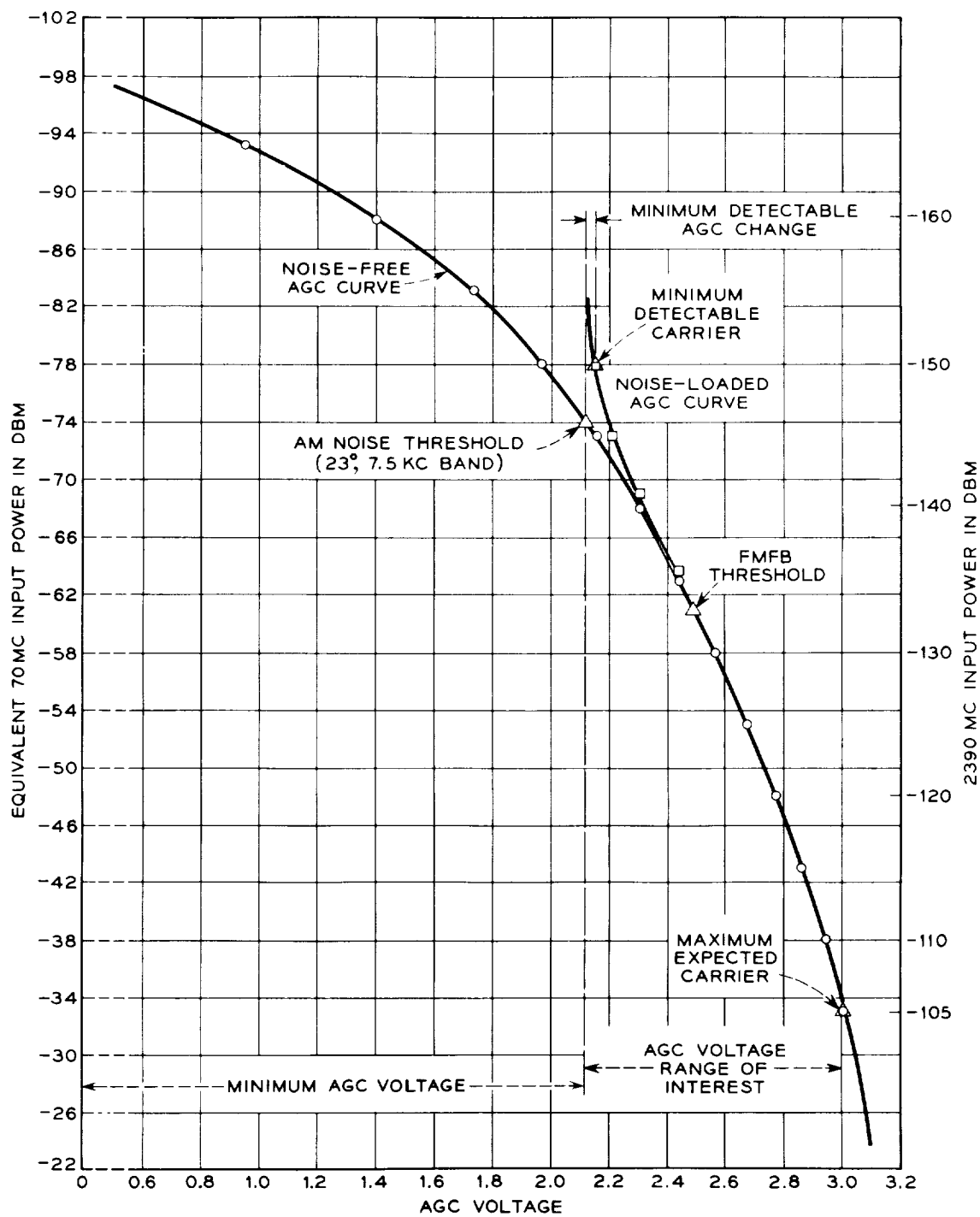


Figure 9 - FMFB demodulator AGC characteristics

the input noise was minimized by pointing the antenna toward the zenith. For reference, the curve on the left in Figure 9 is an AGC characteristic which was obtained by using equivalent 70-Mc carriers that were essentially noise-free. As can be seen, the net gain from the "front end" was adjusted to utilize the region of highest AGC voltage. This placed the AGC "voltage range of interest" in the most linear portion, as shown on the right, and also gave the most nearly constant amplitude at the limiter input. The 2390-Mc AGC characteristic is identical to the noise-free reference for carrier levels well above the threshold.

As the 2390-Mc carrier is decreased below the threshold, the AGC characteristics begin to diverge. The reason for this is that the FM loop loses control, and this causes the receiver to be intermittently detuned. For a correct average VCO tuning and an unmodulated received carrier the AM noise increases, and this in turn increases\* the AGC from the "noise-free" case, in a known and reproducible way, as shown by the right-hand curve in Figure 9. As the 2390-Mc input is decreased well below the threshold, a minimum AGC voltage is reached, as is shown by the sharp vertical rise of the right-hand curve in Figure 9. This limit is due to noise power from the front end; it will now be calculated. Since the FM feedback is ineffective at these levels the demodulator acts like an AM detector. The noise bandwidth of the demodulator AGC circuit is given by the bandwidth when the FM loop is open (Reference 2), and is only 7.5 kc. For a 23°K system temperature the limiting noise power is -146 dbm. As in other AM systems, a somewhat smaller carrier will cause an observable change in the AGC voltage and, as shown in Figure 9, the minimum detectable carrier for this demodulator was -150 dbm. The significance of this was that the carrier could be detected and measured down to the horizon, and that the cross component could be readily monitored during most of each pass.

The AGC "voltage range of interest" of Figure 9 was attenuated, somewhat, and back-biased, in order to use the total recorder chart area as shown by the top recording of Figure 4. The 2390-Mc input carrier power calibrations are shown on the right-hand edge of Figure 9. The overall calibration accuracy was limited mainly by uncertainties of the input carrier powers, and is estimated to be within 0.5 db of nominal. The time constant of the AGC circuit was about 0.02 second; since the typical fades were much slower, none of the fading rates shown on any of the AGC recordings were limited by the recording equipment.

In addition to the measurements of the received carrier power, some noise measurements were made with the overall receiving system in order to verify the audio FM demodulator characteristics. Since the threshold carrier-to-noise power (referred to a 6-kc band) is 14 db, and the average temperature at the zenith 23°K, the minimum threshold carrier power was calculated to be -133 dbm. The actual threshold carrier was found by noting the minimum calibration power required to avoid "popping" in the audio

\*Modulated carriers will decrease the AGC voltage somewhat.

circuit when the antenna was pointed toward the zenith. This turned out to be -133 dbm, as expected.

The quality of the audio circuit was verified in the manner described below. Shortly before a pass a 70-Mc FM test oscillator was temporarily connected to the demodulator input. The carrier level was set equal to that anticipated from the satellite system. The FM (sine wave) deviation was set at the maximum allowed by the demodulator, and the corresponding maximum audio power was measured at the output with a 2B noise set. The audio output noise from the received unmodulated carrier was then measured during the pass. The results were combined to give a reasonable indication of the signal-to-noise ratio. The carrier of the corresponding carrier-to-noise ratio was found from the calibrated AGC voltages, and the noise power (referred to a 6-kc band) was calculated from the observed system temperature. The resulting signal-to-noise ratio versus carrier-to-noise ratio was plotted and found in good agreement with previous laboratory results, as well as with the results predicted from FM theory; these are shown in Figure 27 of Reference 4.

The main characteristics of the receiver are summarized in Table 3.

Table 3  
Over-all Receiver Characteristics

Characteristic	Value
Nominal frequency	2390 Mc
Number of channels	2 (one for each sense of circular polarization)
RF cross coupling (between channels)	-34 db
Audio bandwidth (each channel)	0.2 to 3 kc
Maximum FM deviation	$\pm 30$ kc
Minimum system temperature	$21 \pm 1^\circ\text{K}^*$
Minimum Threshold carrier power	-133 dbm
Minimum detectable carrier power	-150 dbm
Carrier Calibration Range	-110 dbm to -150 dbm
Time constant of carrier recordings	0.02 second
Carrier Calibration Accuracy	(from $\pm 0.5$ db above threshold to $\pm 2$ db well below threshold)

\* $17.25 \pm 1^\circ\text{K}$  without a paramp standby provision.

## EXPERIMENTAL RESULTS

The main experimental results, which include complete data of the west-to-east satellite systems, are given by the four-channel pen recordings shown in Figures 10 through 21 of Reference 4. Two high-quality voice circuits, with signal-to-noise ratios greater than 36 db, were also available from the receiver whenever the resulting ratio

of received carrier-to-noise power (referred to a 6-kc band) exceeded 14 db. These experimental results are shown in Figure 27 of Reference 4.

A locus of the minimum carrier level required during a typical pass (for the critical 14-db carrier-to-noise ratio) is shown in the top recording of Figure 4. For convenience, this is superimposed on a recording of a carrier received from Goldstone under good tracking conditions. The minimum carrier level required when a paramp was used instead of a maser is also shown. These plots verified the fact that a good voice circuit could be achieved with the paramp under modest carrier fading conditions (which are shown) and that the fading margin for a good voice circuit using the maser was about 16 db over most of a pass. (This is significant, since the consistent maximum fading due to the balloon\* turned out to be only 10 db.)

When corrections were made for some known transmitter, refraction, and tracking errors, the calibrated carrier level recordings verified that the entire communication system was working properly, and that the path losses were characterized by the propagation laws of free space. The recordings also measured the random variations that occurred during every operational pass and the random decreases in average level that occurred from pass to pass.

Certain observed characteristics of the carrier level recordings were also used to identify some otherwise unknown transmitter tracking errors. The key characteristics were: (1) a much more jagged than normal carrier level recording, especially in conjunction with a lower than normal average level;\* (2) an anomalous increase in carrier level adjacent to a gross pointing error; † and (3) a period of decreased main carrier level, with simultaneous increase in the average cross-component level. ‡ These additional clues made it possible to eliminate some questionable data in order to evaluate more accurately the reflection characteristics of the balloon.

The recorded system temperatures verified that the background sky temperature varied as anticipated, and that the isolated sources of large sky temperature were seldom encountered. The temperature recordings also showed that other sources, such as lightning, clouds, nearby radars, and radio stars occasionally added to the system temperature, but only by a few degrees.

## ACKNOWLEDGMENTS

Several people, in addition to those already mentioned, made significant contributions to this receiver. The complex assembly and testing could not have been accomplished on

\*Shown in Pass 1086, after 0944 GMT (Figure 20 of Reference 4).

† See Pass 229 at 0453:30 GMT (Figure 15 of Reference 4).

‡ See Pass 60 at 0756:50 GMT (Figure 4 of this paper).



schedule without the timely and generous aid of W. W. Snell and H. A. Anderson. Other timely aid was provided by H. E. Keller, F. A. Dunn, R. A. Semplak, R. H. Turrin, and W. E. Legg. The precision square-law detectors (with large output voltages), the precision system temperature measurements (needed to determine the sky temperature), and the automatic nitrogen transfer system are all due to the work of W. W. Snell. Aid in operating the receiver was provided by E. L. Frantsvog, R. A. Desmond, and W. F. Bodtmann. After the Echo I experiments were concluded, the waveguide losses were precisely measured by G. S. Axeling.

#### REFERENCES

1. Ruthroff, C. L., and Jakes, W. C., Jr., "Project Echo — System Calculations," Bell System Tech. J. 40(4):1029-1039, July 1961; also NASA Technical Note D-1128, in publication, 1961
2. Ruthroff, C. L., "Project Echo — FM Demodulators with Negative Feedback," Bell System Tech. J. 40(4):1149-1156, July 1961; also NASA Technical Note D-1134, 1961
3. De Grasse, R. W., Hogg, D. C., Ohm, E. A., and Scovil, H. E. D., "Ultra-Low-Noise Antenna and Receiver Combination for Satellite or Space Communication," Proc. Nat. Elect. Conf. 15:370-379, 1959
4. Jakes, W. C., Jr., "Participation of Bell Telephone Laboratories in Project Echo and Experimental Results," Bell System Tech. J. 40(4):975-1028, July 1961; also NASA Technical Note D-1127, in publication, 1961
5. Crawford, A. B., Hogg, D. C., and Hunt, L. E., "Project Echo — Horn Reflector Antenna for Space Communication," Bell System Tech. J. 40(4):1095-1116, July 1961; also NASA Technical Note D-1131, in publication 1961
6. Schelkunoff, S. A., "Electromagnetic Waves," New York: Van Nostrand, 1943, pp. 260, 269, 327, 390
7. Mumford, W. W., unpublished manuscript
8. Bolinder, F., "Fourier Transforms in the Theory of Inhomogeneous Transmission Lines," Stockholm: Trans. Royal Inst. Tech., No. 48, 1951
9. Beck, A. C., and Dawson, R. W., "Conductivity Measurements at Microwave Frequencies," Proc. I.R.E. 38(10):1181-1190, October 1950
10. De Grasse, R. W., Kostelnick, J. J., and Scovil, H. E. D., "Project Echo — Dual Channel 2390-Mc Traveling Wave Maser," Bell System Tech. J. 40(4):1117-1127, July 1961; also NASA Technical Note D-1132, in publication, 1961

11. Kibler, L. U., "Project Echo — Standby Receiver System," Bell System Tech. J. 40(4):1129-1147, July 1961; also NASA Technical Note D-1133, in publication, 1961

### Front-End Tuning

D-1130

In order to maintain the low inherent system temperature and calibrate the receiver before and after each satellite pass, a fast, easy-to-use measuring system was required. Such a system was interconnected to both channels of the receiver; the connections to a single channel are shown in Figure A1. Front-end RF test signals were generated in the antenna cab and inserted into the receiver via an 18-db waveguide directional coupler. The IF results were then readily monitored and/or measured by means of a permanently installed IF coupling network.

All required signal levels were achieved by attenuating a known reference power with coaxial attenuators, as shown in the lower left of Figure A1. Since the calibrated input carriers were as low as -150 dbm, shielding precautions were required in order to reduce RF leakage from the test equipment to the input waveguide. The multiple chokes used

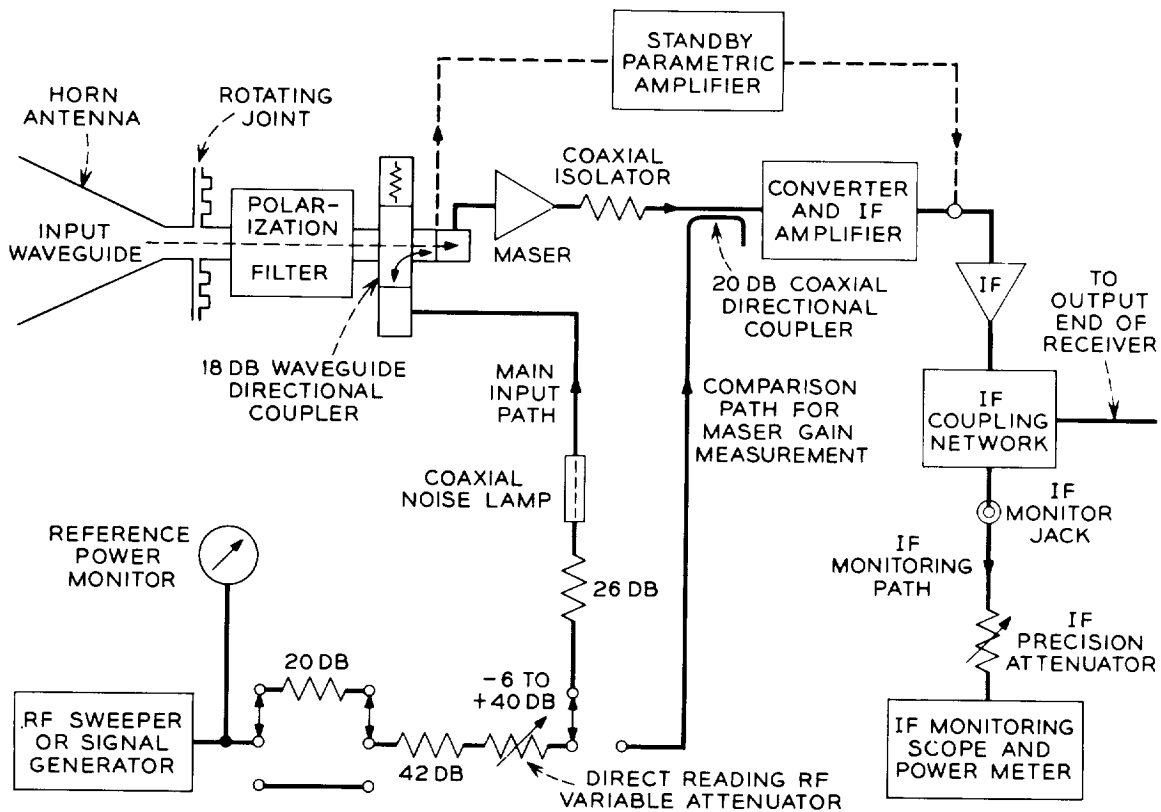


Figure A1 - Front-end measuring system

around the waveguide rotating joint and the well-shielded General Radio connectors used for coaxial attenuator switching were highly effective features. The attenuator values were selected so as to prevent (after proper switching) erroneous results due to saturation effects or poor carrier-to-noise ratios. The selected values also allowed the use of a direct-reading General Radio RF attenuator for the entire input carrier calibration range.

The first tuning step was to optimize the bandpass characteristic of either the maser or the paramp, using a swept signal well above the noise. The maser gain was then found by comparing the previously known input carrier power with that required when it was inserted after the maser (via the permanently installed 20 db coaxial directional coupler). The monitored IF power was held constant for this measurement. Alternatively, paramp gain was found by inserting a known input carrier and comparing this to the 70-Mc power in the IF monitoring jack. After achieving the normal gain and frequency range, the system temperature was checked as shown in Appendix B. The final step was to furnish known input carriers to calibrate the AGC voltages (about 10 minutes before each pass). As can be seen in Figure A1, this was done by simply adjusting the direct-reading RF attenuator when the fixed attenuators were connected as shown.

## Appendix B

## System Temperature Measurements

After the antenna had been pointed toward the zenith, data for the system temperature were found by coupling excess noise from an argon noise lamp into the input waveguide as shown in Figure A1 of Appendix A and then measuring the increase in IF output power. The system temperature was then:

$$T_{\text{system}} = \frac{T_H L_{\text{coax}} L_{\text{coupler}}}{Y - 1} ,$$

where  $T_H$  is the excess noise at the output terminal of the coaxial noise lamp,  $L_{\text{coax}}$  is the insertion loss between the noise lamp and the directional coupler,  $L_{\text{coupler}}$  is the coupling loss of the waveguide directional coupler, and  $Y$  is the ratio of lamp "on" to lamp "off" power at the IF monitor jack.  $T_H$  was calculated<sup>1</sup> using the measured<sup>2</sup> electron temperature of a similar argon lamp ( $10,500 \pm 265^\circ\text{K}$  at 6 kMc), and the measured insertion losses (15.5 db "on" and 2.4 db "off") for this particular coaxial noise lamp mount. The result was  $T_H = 8360 \pm 225^\circ\text{K}$ . The measured insertion loss of the coaxial line was 1.31 db and the measured coupling of the directional coupler was  $18.15 \pm 0.15$  db. Therefore, upon solving the numerator, the total excess temperature coupled into the waveguide,  $T_{\text{coupled}}$ , was  $94.6 \pm 6^\circ\text{K}$ , and

$$T_{\text{system}} = \left( \frac{94.6 \pm 6}{Y - 1} \right) ^\circ\text{K}.$$

Using a paramp, the observed values of  $Y$  varied from 1.30 to 1.35. The corresponding paramp system temperatures are  $270^\circ$  and  $315^\circ\text{K}$ . Using a maser,  $Y$  was typically about 5 and therefore the maser system temperature was about  $23^\circ\text{K}$ . A 27-db coupler could have been used instead of the 18-db coupler to reduce  $Y$  to a still acceptable value of 1.65. This would also have reduced the system temperature  $3.75^\circ\text{K}$ . For the paramp, however,  $Y$  would then have been too small for a meaningful measurement. The 18-db couplers were therefore retained in service to provide a standby measuring technique for the paramp system temperature. The maser system temperature results for other antenna beam elevations are shown by the middle curve of Figure 2 in the body of this report.

<sup>1</sup>White, W. D., and Green, J. G., "On the Effective Noise Temperature of Gas Discharge Noise Generators," Proc. I.R.E. 44(7):939, July 1956

<sup>2</sup>DeGrasse, R. W., Hogg, D. C., Ohm, E. A., and Scovil, H. E. D., "Ultra-Low-Noise Antenna and Receiver Combination for Satellite or Space Communication," Proc. Nat. Elect. Conf. 15:370-379, 1959

## Appendix C

## Sky Temperature

Since the sky temperature seen by a narrow beam antenna is proportional to the length of antenna beam passing through each layer of atmosphere, the sky temperature at the zenith, whatever its value, will approximately double when the antenna beam is lowered to an elevation of 30 degrees. It will redouble at 14.5 degrees, quadruple at 7.2 degrees, and so forth, as given by

$$T_{\text{sky at } \theta_z} \approx \frac{T_{\text{sky at } \theta_z}}{\sin \theta}, \quad \theta > 5^\circ, \quad (\text{C1})$$

where  $\theta$  is the elevation of the antenna beam above the horizon and  $\theta_z$  is an elevation of 90 degrees. Only a narrow range of sky temperatures, when doubled, redoubled, etc. (and added to a constant), will match the observed maser system temperatures. Following this restraining principle, it can be shown that the sky temperature at the zenith can be determined from the maser system temperatures and the theoretical ratio,  $N$ , of  $T_{\text{sky at } \theta}$  to  $T_{\text{sky at } \theta_z}$ . This result is given by:

$$T_{\text{sky at } \theta_z} = \frac{T_{\text{system at } \theta} - T_{\text{system at } \theta_z}}{N - 1}, \quad (\text{C2})$$

where  $N$ , derived from Equation C1, is:

$$N = \frac{T_{\text{sky at } \theta}}{T_{\text{sky at } \theta_z}} \approx \frac{1}{\sin \theta}. \quad (\text{C3})$$

For improved accuracy, more exact values of  $N$ , which take into account the curvature of the earth's atmosphere, should be used (these ratios can be found from the results of a theoretical derivation of sky temperature<sup>1</sup>); random experimental limits should be allowed for; and the required use of zenith system data should be eliminated. A more general form of Equation C2 was therefore derived which allows these advantages:

$$T_{\text{sky at } \theta_z} = \frac{\left( \frac{T_{\text{max at } \theta} + T_{\text{min at } \theta}}{2} \right) - \left( \frac{T_{\text{max at } \theta_0} + T_{\text{min at } \theta_0}}{2} \right)}{N_\theta - N_{\theta_0}}, \quad (\text{C4})$$

where  $T_{\text{max}}$  and  $T_{\text{min}}$  are the respective temperature limits (after allowing for random experimental errors) for two elevations,  $\theta$  and  $\theta_0$ ; and  $N_\theta$  and  $N_{\theta_0}$  are the theoretical

<sup>1</sup>Hogg, D. C., "Effective Antenna Temperature Due to Oxygen and Water Vapor in the Atmosphere," J. Appl. Phys. 30(9):1417-1419, September 1959

sky temperature ratios, defined in Equation C3, for these two elevations. For greatest accuracy, many different widely separated combinations of  $\theta_0$  and  $\theta$  must be used and great care must be exercised to allow for random increases in system temperature due to the antenna side lobes.

It can also be shown that the limits of the sky temperature are given by:

$$\Delta T_{\text{sky at } \theta_z} = \pm \frac{\left( \frac{T_{\text{max at } \theta} - T_{\text{min at } \theta}}{2} \right) + \left( \frac{T_{\text{max at } \theta_0} - T_{\text{min at } \theta_0}}{2} \right)}{N_\theta - N_{\theta_0}} \quad (\text{C5})$$

By selecting measured maser system temperatures from Figure 2 (in the body of this report) for many pairs of elevation angles down to 5 degrees, the sky temperature at the zenith was found to be

$$T_{\text{sky}} = 2.30 \pm 0.2^\circ\text{K}.$$

This was in good agreement with theory, which predicted a value of  $2.4^\circ\text{K}$ .

## Appendix D

## Liquid Nitrogen

The outer dewar of the maser had to be kept cold with liquid nitrogen and, due to "boil-off", the liquid in the dewar had to be replenished every 12 hours. Figure D1 shows how batches of liquid were automatically supplied for periods of five days. Since it was too heavy and bulky to go into the antenna cab, the 100-liter supply container was located on the rotating base of the antenna. The boil-off losses of the resulting long transfer line were kept within reason by the use of thin-wall stainless-steel tubing surrounded by an insulating foam.

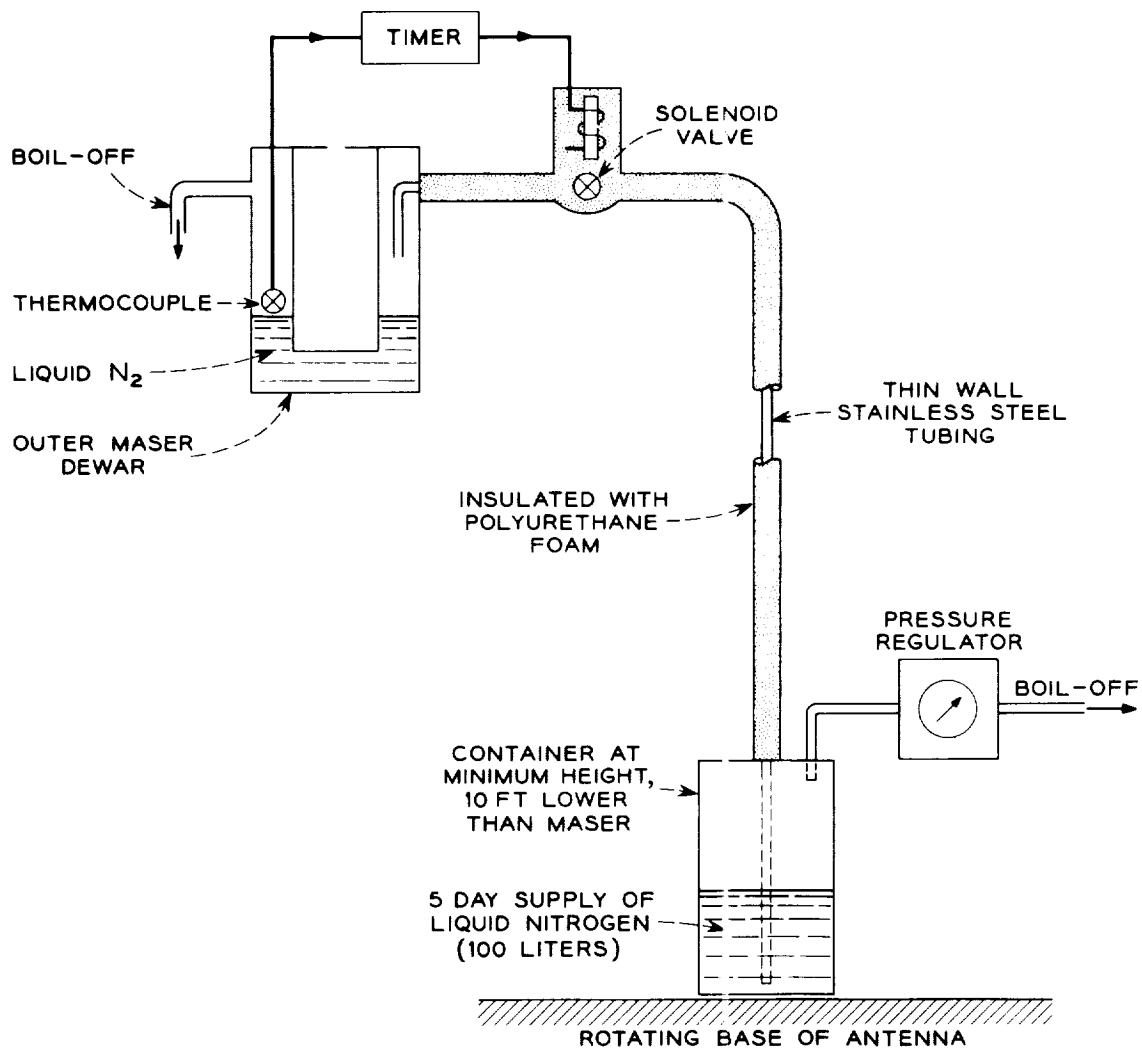


Figure D1 - Automatic liquid nitrogen transfer system



The sensing device of the system was a thermocouple placed in the outer maser dewar which sent a signal to the timer when liquid was required. The timer kept the solenoid valve open just long enough to fill the dewar. The liquid was pumped through the open solenoid valve at a predictable rate by the storage container "back pressure." This was stabilized by the pressure regulator, which could also adjust the back pressure for different flow rates.

Although preliminary cooling of the line (and valve) during the transfer process boiled off some nitrogen, changing of output flow from warm to cold gas and then increasing the quantities of liquid greatly reduced the thermal shock on the dewar. This system, designed and built by W. W. Snell, is highly recommended for automatic nitrogen servicing.

## Appendix E

**Liquid Helium**

In order to operate the maser, the inner maser dewar had to be cooled with liquid helium. Because liquid helium has an extremely low temperature and a low specific heat, special vacuum-insulated storage and handling facilities were required to prevent excessive "boil-off" losses. The resulting storage containers were therefore quite heavy and the liquid had to be "transferred" (from storage to another dewar) in batches via vacuum-insulated transfer lines.

For daily maser operations large quantities of liquid were required, and these could not be supplied locally. The necessary amounts were accordingly shuttled every fourth day from Tonawanda, New York, in two special 100-liter containers. This type of "super-insulated" container was selected because it could conveniently supply the maser for four days from a platform on the rotating base of the antenna. This eliminated the need for daily heavy lifting, and indeed all lifting, since the platform could be easily reached by truck. Another convenient feature of this container was that liquid nitrogen servicing was not required. As a result, the container was relatively light (for its capacity) and one person could easily load it on the antenna.

The helium transfer system is shown in Figure E1. The transfer line was flexible, so that it could be easily connected to the storage containers on the lower end (this starts the transfer) and easily inserted into the maser dewar on the other (after the line was very cold). The liquid was pumped by storage container back pressure. The rate of liquid flow into the line was monitored by watching the scale weight, and the boil-off rate was monitored by watching the flow meter. If these readings were abnormal the transfer was stopped (by disconnecting the flexible line from the storage container) to find the source of trouble. Otherwise, the transfer was continued until the scale reached a predetermined cutoff weight.

Cutoff weight was a function of the initial weight of the container and the length of time it was desired to operate the maser. The operating times for different quantities of liquid are shown in Figure E2. The time was determined from the beginning of flow from the storage container. As can be seen, these are also a function of the initial temperature of the dewar. The maximum operating time was over 18 hours, well in excess of the 12 hours required for a series of Echo passes. For daily transfers 12 hours could be obtained using only 14 liters of liquid. The normal objective, which included a 1-liter safety factor, was 15 liters. Since the corresponding weight was 4-1/4 pounds, the normal cutoff weight of the storage container was selected to be about 4-1/4 pounds less than its initial weight.

After the transfer was completed the transfer tube was removed from the maser, (to eliminate the tube as a heat leak), and the aperture was sealed with a stopper. The liquid

D-1130

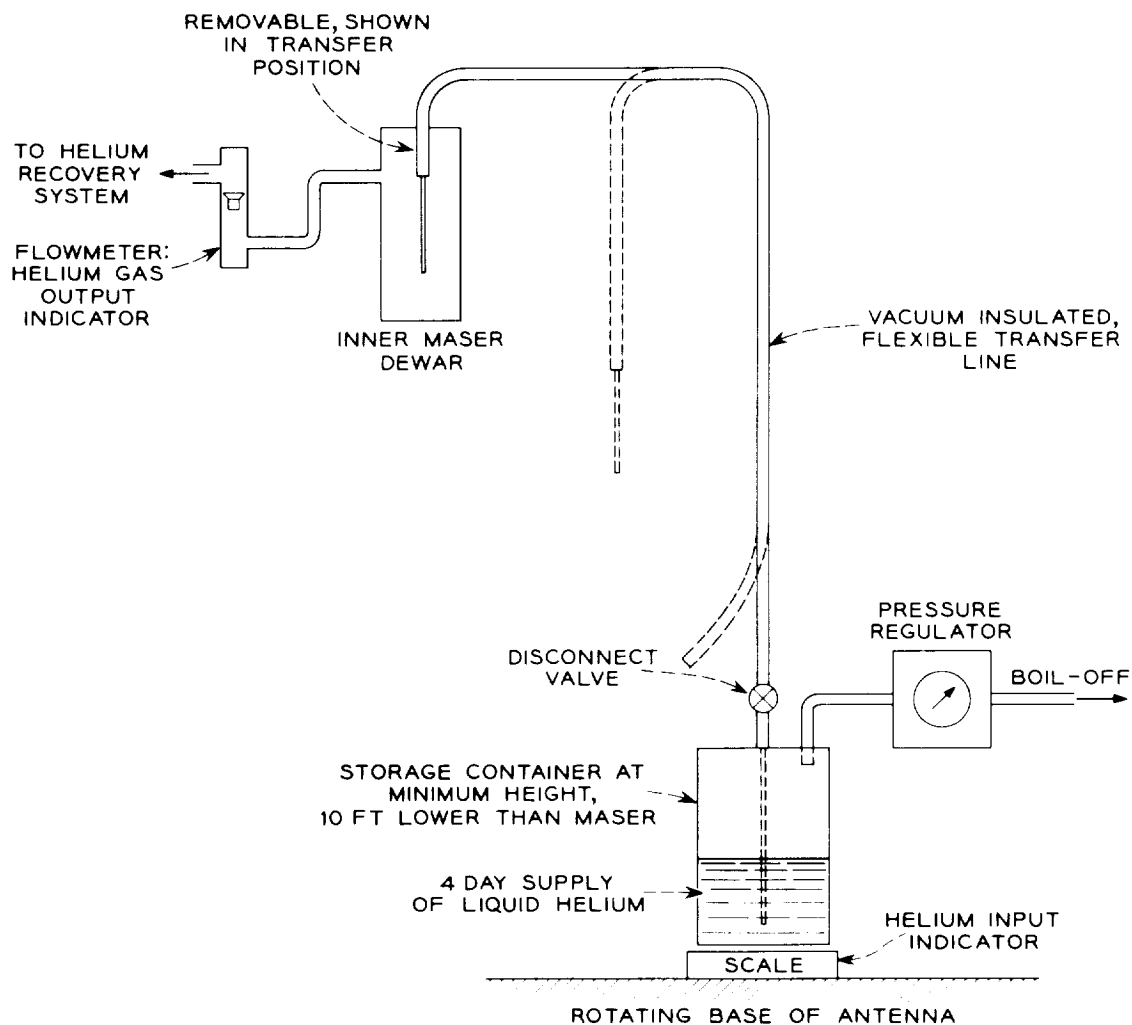


Figure E1 - Liquid helium transfer system

helium in the maser dewar was then "pumped down" (with a vacuum pump) to reduce the maser temperature still further. The pressure declined smoothly until the "lambda" pressure was reached; it then declined at a much slower rate. By noting the time from the start of the "pump down" to the lambda point and comparing this with previous data, the maser running time could be reliably predicted to within a half hour or so. The vacuum pump, incidentally, was located at the base of the antenna in order to rid the cab of its noise and vibration.

Since the receiver was planned during a period of helium shortage, a gas recovery system was included as a conservation measure. The boil-off from the helium transfer

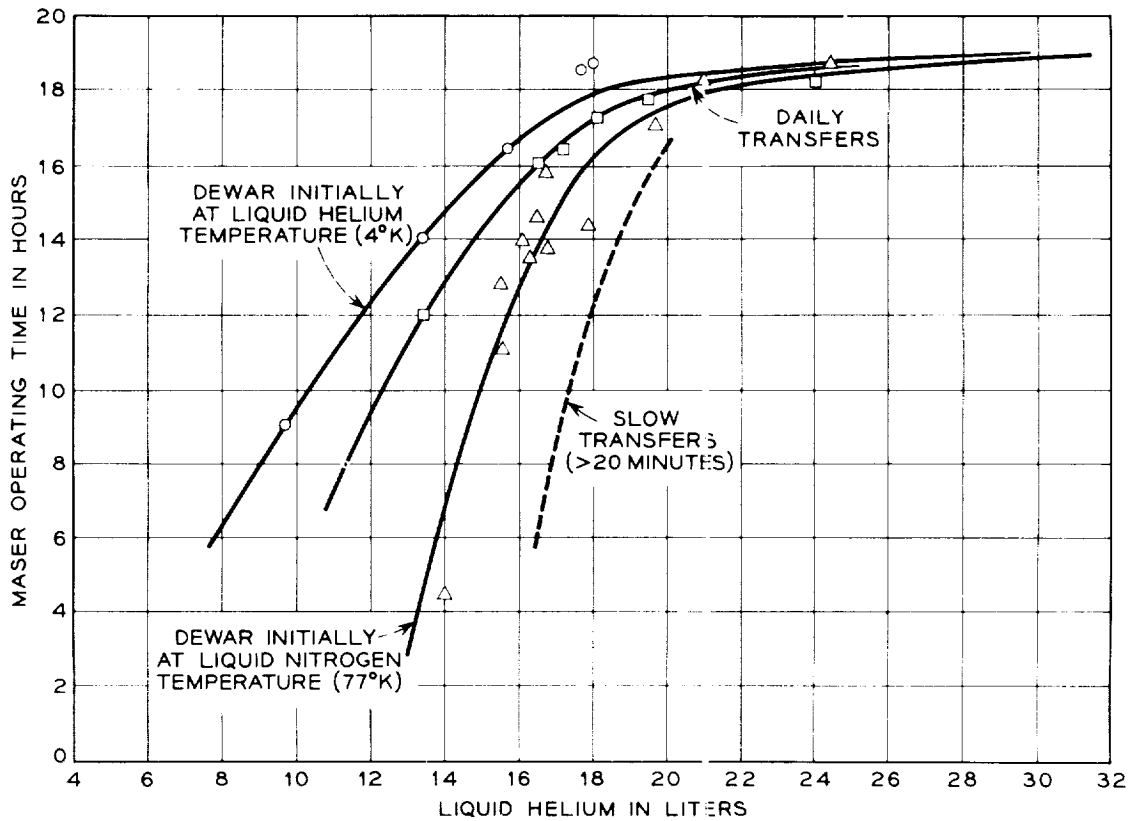


Figure E2 - Liquid helium required vs. maser operating time

and the exhaust from the vacuum pump were piped to the recovery system (in a nearby building) via a rotating joint on the vertical axis of the antenna mount. Although the integrated boil-off rate exceeded the storage and compression capacity by a large factor, excess time was short, and 75 percent of the available gas could be recovered and purified.